Remote Sensing of Environment 196 (2017) 1–12

Contents lists available at ScienceDirect

Remote Sensing of Environment

journal homepage: www.elsevier.com/locate/rse

A snow-free vegetation index for improved monitoring of vegetation spring green-up date in deciduous ecosystems

Cong Wang [a,b], Jin Chen [a,*], Jin Wu [c], Yanhong Tang [d], Peijun Shi [a], T. Andrew Black [e], Kai Zhu [b,f]

[a] State Key Laboratory of Earth Surface Processes and Resource Ecology, Beijing Normal University, Beijing, 100875, China
[b] Department of Biology, University of Texas at Arlington, 701 S. Nedderman Drive, Arlington, TX 76019, USA
[c] Environmental and Climate Sciences Department, Brookhaven National Laboratory, Upton, New York 11973, USA
[d] College of Urban and Environmental Sciences, Peking University, Beijing 100871, China
[e] Faculty of Land and Food Systems, University of British Columbia, 2357 Main Mall, Vancouver, BC V6T 1Z4, Canada
[f] Department of BioSciences, Rice University, 6100 Main Street, Houston, TX 77005, USA

ARTICLE INFO

Article history:
Received 15 September 2016
Received in revised form 24 April 2017
Accepted 28 April 2017
Available online 5 May 2017

Keywords:
Vegetation phenology
Green-up date
Remote sensing
Snowmelt
NDPI
Climate change

ABSTRACT

Vegetative spring green-up date (GUD), an indicator of plants' sensitivity to climate change, exerts an important influence on biogeochemical cycles. Conventionally, large-scale monitoring of spring phenology is primarily detected by satellite-based vegetation indices (VIs), e.g. the Normalized Difference Vegetation Index (NDVI). However, these indices have long been criticized, as the derived GUD can be biased by snowmelt. To minimize the snowmelt effect in monitoring spring phenology, we developed a new index, Normalized Difference Phenology Index (NDPI), which is a 3-band VI, designed to best contrast vegetation from the background (i.e. soil and snow in this study) as well as to minimize the difference among the backgrounds. We examined the rigorousness of NDPI in three ways. First, we conducted mathematical simulations to show that NDPI is mathematically robust and performs superior to NDVI for differentiating vegetation from the background, theoretically justifying NDPI for spring phenology monitoring. Second, we applied NDPI using MODIS land surface reflectance products to real vegetative ecosystems of three in-situ PhenoCam sites. Our results show that, despite large snow cover in the winter and snowmelt process in the spring, the temporal trajectories of NDPI closely track the vegetation green-up events. Finally, we applied NDPI to 11 eddy-covariance tower sites, spanning large gradients in latitude and vegetation types in deciduous ecosystems, using the same MODIS products. Our results suggest that the GUD derived by using NDPI is consistent with daily gross primary production (GPP) derived GUD, with R (Spearman's correlation) = 0.93, Bias = 2.90 days, and RMSE (the root mean square error) = 7.75 days, which outcompetes the snow removed NDVI approach, with R = 0.90, Bias = 7.34 days, and RMSE = 10.91 days. We concluded that our newly-developed NDPI is robust to snowmelt effect and is a reliable approach for monitoring spring green-up in deciduous ecosystems.

1. Introduction

Vegetative spring green-up date (GUD) is a sensitive indicator of temperate and boreal ecosystems responding to global climate change (Wolkovich et al., 2012; Fu et al., 2016; Menzel and Fabian, 1999; Parmesan and Yohe, 2003; Wang et al., 2016). A number of studies have reported that the start of spring is occurring earlier in the recent decades in temperate and boreal ecosystems in the Northern Hemisphere (e.g. Buitenwerf et al., 2015; Myneni et al., 1997; Zhou et al., 2001). This shift in phenology exerts an important influence on large-scale biogeochemical cycles (Richardson et al., 2010; Xia et al., 2015). For example, Richardson et al. (2009) showed that earlier spring onset resulted in higher annual gross primary productivity (GPP) at two forest sites in the United States. However, a reliable approach for monitoring spring phenology in these ecosystems is still lacking.

For decades, satellite remote sensing has offered an attractive tool for large-scale motoring of vegetative status (Buitenwerf et al., 2015; Wang et al., 2015). The most widely used remote sensing product is the Normalized Difference Vegetation Index (NDVI). It uses two reflectance spectral bands and ratios them to provide an estimate of canopy greenness, a composite property of both leaf-level (leaf intercellular structure and biochemical compostion) and canopy-level (canopy leaf area and structure) properties. In general, NDVI is a good indicator of

* Corresponding author.
E-mail address: chenjin@bnu.edu.cn (J. Chen).

http://dx.doi.org/10.1016/j.rse.2017.04.031
0034-4257/

plant growth status (Pettorelli et al., 2005), and is thus widely used for phenology monitoring.

However, satellite-derived NDVI can be affected by two natural processes of snowmelt and vegetative growth in spring, as these two processes can both increase NDVI value. As a result, the derived vegetation phenology (e.g. GUD) using the NDVI approach can be contaminated by the snowmelt (Delbart et al., 2005; Shabanov et al., 2002). This snowmelt effect, without fair justifications, can even lead to the misinterpretation of climate impact on vegetative phenology. For example, Zhang et al. (2013) found that GUD in the Tibetan Plateau advanced continuously from 1982 to 2011 by using three long-term NDVI time series. However, more recent studies (e.g. Shen et al., 2013; Wang et al., 2013) argued that the detected spring phenological trend in the Tibetan Plateau might be due to the artifact caused by declining snow cover. Therefore, it urgently calls for a new, more accurate approach for monitoring spring vegetation phenology, which is robust to the snowmelt effect (White et al., 2005).

To minimize the snowmelt artifact on NDVI-detected GUD, a number of methods have been proposed in the past decades. However, a mathematically rigorous and generalized method is still lacking. An important prerequisite for most previous approaches is the prior knowledge of temporal changes of snow cover. This prior knowledge can either be empirically determined (Beck et al., 2006; Karlsen et al., 2014), or rely on auxiliary data (Cao et al., 2015; Wang et al., 2015) which limits the general applicability of these approaches.

Several other vegetation indices (VIs) to account for the snowmelt effect have also been proposed and examined, but all these VIs are subject to various issues limiting their effectiveness. For example, some remote sensing scientists advocated the use of the Normalized Difference Infrared Index (NDII) (also referred to as the Normalized Difference Water Index (NDWI)) which includes the spectral band (shortwave-infrared) sensitive to foliar water content, for vegetative phenology monitoring (e.g. Delbart et al., 2005; Delbart et al., 2006; Dunn and de Beurs, 2011). This is because NDII increases with vegetation growth but decreases with snowmelt, and thus it is promising in being able to decouple snowmelt from vegetation growth. However, the NDII approach is disadvantageous for those regions where snowmelt and the start of vegetative growth occur at the same period (Gonsamo et al., 2012). In some burned areas, NDII is also found to be not sensitive to vegetation growth (Peckham et al., 2008). Phenology Index (PI), a composite VI of NDVI and NDII, was proposed as an alternative approach to overcome the drawback of using NDII alone (Gonsamo et al., 2012). The issue of using PI is that it is not sensitive to vegetation growth when the vegetation is sparse. More recently, (Thompson et al., 2015) characterized the vegetation phenology by constructing a phase-spaces using both NDVI and NDII. Days of the year (DOYs) for a pixel are classified as one of two types, i.e. snow-free phase and snow-covered phase, and the GUD is defined as the date when the pixel entered and remained in the snow-free phase for no <10 days without returning to the snow-covered phase. This method, however, is somewhat complex and would fail to estimate a consistent phenological time series for the areas where snow cover occasionally happens in between years (e.g. the site CN-Hab in this study).

In this study, we aim to develop a new VI that is resistant to snowmelt and can more accurately monitor spring phenology for snow covered regions. The newly developed VI is the Normalized Difference Phenology Index (NDPI), which is a 3-band VI, using the spectral signal from red, near-infrared (NIR) and shortwave-infrared (SWIR) bands respectively (as used in NDVI and NDII). To evaluate the robustness and performance of the new index in detecting GUD, we firstly performed mathematical simulations and then applied NDPI to real vegetative ecosystems using MODIS land surface reflectance products, validated by using observations from three in-situ PhenoCam sites, and 11 eddy-covariance (EC) flux sites. We show that NDPI is robust to snowmelt and can indicate the GUD in spring better than other VIs (e.g. NDVI) in snow covered regions, especially in deciduous ecosystems.

2. Methodology and data

2.1. Definition of vegetation indices (VIs)

2.1.1. Normalized Difference Vegetation Index (NDVI)

NDVI is calculated from the red (ρ_{red}) and near-infrared (NIR, ρ_{NIR}) band reflectance as follows (Asrar et al., 1984):

$$NDVI = \frac{\rho_{NIR} - \rho_{red}}{\rho_{NIR} + \rho_{red}} \quad (1)$$

The red band is located in the strong chlorophyll absorption region (about 600–700 nm), and the NIR band is located in the high reflectance plateau which is related to the leaf internal structure (about 700–1100 nm). NDVI is correlated with the leaf area index (LAI) and the absorption of photosynthetically active radiation by the canopy (Asrar et al., 1984).

2.1.2. Normalized Difference Infrared Index (NDII)

NDII (NDWI) has a similar definition to that of NDVI but replaces ρ_{red} with the shortwave-infrared radiation (SWIR, about 1300–2700 nm) reflectance (ρ_{SWIR}, Hardisky et al., 1983):

$$NDII = \frac{\rho_{NIR} - \rho_{SWIR}}{\rho_{NIR} + \rho_{SWIR}} \quad (2)$$

A large absorption by leaf water is observed in the SWIR bandwidth and thus this index reflects the effect of leaf water content (Fensholt and Sandholt, 2003). The exact wavelength of SWIR varies slightly depending on researchers. For instance, the wavelength of SWIR was defined as 1240 nm in Gao (1996), and 1580–1750 nm in Xiao et al. (2002). Despite the difference in the SWIR wavelength used, they accomplish similar things with each other.

2.1.3. Phenology Index (PI)

Gonsamo et al. (2012) proposed the PI which is a complex combination of NDVI and NDII:

$$PI = \begin{cases} 0, & if\ NDVI\ or\ NDII<0 \\ NDVI^2 - NDII^2 & \\ 0, & if\ PI<0 \end{cases} \quad (3)$$

PI was designed to improve the capability of monitoring vegetation phenology by removing the wetness and brightness effects from greenness of land surface, especially the confounding effect of the snow (Gonsamo et al., 2012). The authors constrained the variance of PI caused by snow dynamics by assigning zero to PI for some conditions.

2.1.4. Normalized Difference Phenology Index (NDPI)

We proposed a new index, NDPI, motived by Gonsamo et al. (2012). NDPI directly employs the red, NIR and SWIR bandwidths. The most desirable property of NDPI is to be free of the snowmelt effect but is sensitive to initial vegetation growth during the spring green-up period. To achieve this goal, we firstly examined spectral reflectance curves of typical main components of the land surface (Fig. 1). The reflectance of both soil and snow varies monotonically from red to SWIR wavelengths (increasing for soil; decreasing for snow). For vegetation, however, the reflectance of NIR bandwidth is high while the reflectance of the red and SWIR bandwidth are low. To make use of this unique feature, we first define a new red-SWIR reflectance (ρ_{red}^{SWIR}) as the weighted sum of the red and SWIR reflectance in order to minimize the difference between soil and snow that are the main components of the land surface in the non-growing season:

$$\rho_{red}^{SWIR} = \alpha \times \rho_{red} + (1-\alpha) \times \rho_{SWIR} \quad (4)$$

where α is a weighting coefficient which must be determined, and it is

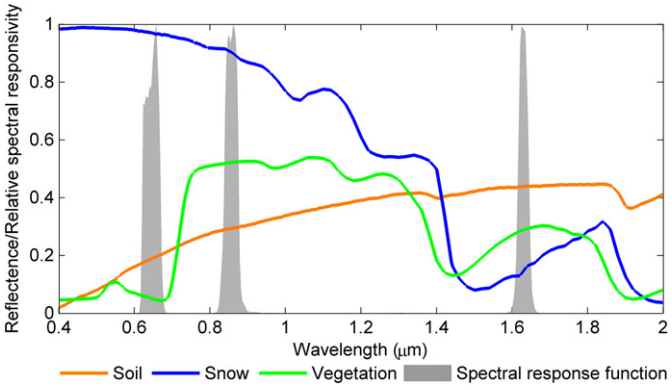

Fig. 1. Spectral reflectance curves from the Aster Spectral Library and the spectral response function of MODIS. Each reflectance curve is an average of spectrum types listed in Table S1. The gray shadow shows the spectral response function for red, near-infrared and shortwave-infrared spectral bands of MODIS.

expected to have a value such that the ρ_{red}^{SWIR} for soil and snow could be close to their respective ρ NIR.

Litters are not separately considered here because it shares similar spectral curve with soil (Nagler et al., 2000). The ρ_{red}^{SWIR} is small for vegetation, because vegetation has a small reflectance in both red and SWIR bandwidths. We then use the 'normalized difference' form to construct NDPI as follows:

$$NDPI = \frac{\rho_{NIR} - \rho_{red}^{SWIR}}{\rho_{NIR} + \rho_{red}^{SWIR}} \quad (5)$$

As expected, with an appropriate value of α, NDPI value is small for soil and snow, but large for vegetation. When α equals 0 and 1, NDPI converges to NDII and NDVI, respectively.

To obtain the optimal α, spectral reflectance curves of 25 soil, 4 snow and 3 vegetation types were selected from the Aster Spectral Library (Table S1, Baldridge et al., 2009). According to the spectral response functions of MODIS band1 (red, 620–670 nm), band2 (NIR, 841–876 nm) and band6 (SWIR, 1628–1652 nm), the values of NDPI with different α's from 0.0 to 1.0 with 0.01 interval were calculated as shown in Fig. 2. When α is set to 0.74, soil and snow achieve similar NDPI values close to 0.1, whereas vegetation achieves a larger value close to 0.6. It suggests that NDPI can make a sharp contrast between vegetation and soil or snow. More importantly, we found that this value of α also results in the minimal variance of NDPI of the 29 soil and snow spectra, indicating that NDPI is insensitive to different soil and snow types. Accordingly, we decided on the value of α to be 0.74 in this study so that NDPI is calculated as follows:

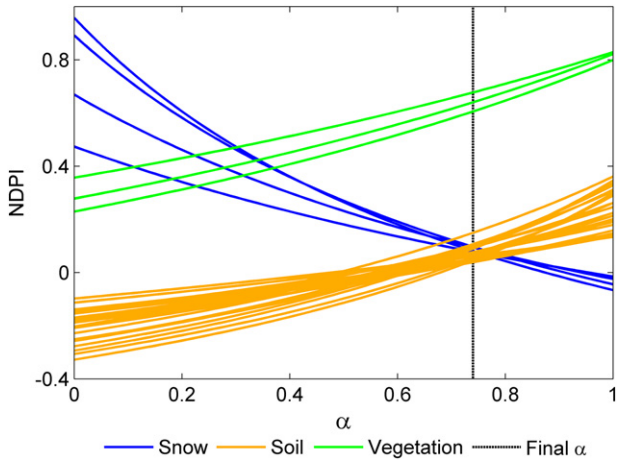

Fig. 2. NDPI values of snow, soil and vegetation with different values of α. The dashed line shows the final α used in this study.

$$NDPI = \frac{\rho_{NIR} - (\alpha \times \rho_{red} + (1-\alpha) \times \rho_{SWIR})}{\rho_{NIR} + (\alpha \times \rho_{red} + (1-\alpha) \times \rho_{SWIR})} = \frac{\rho_{NIR} - (0.74 \times \rho_{red} + (0.26 \times \rho_{SWIR})}{\rho_{NIR} + (0.74 \times \rho_{red} + (0.26 \times \rho_{SWIR})} \quad (6)$$

2.2. Simulation experiments

We simulated 3 typical scenarios to test how snowmelt influences the detection of GUD from different VI time series. In these scenarios, with the assumption that the reflectance spectrum of a pixel comprising three components (snow, soil, and vegetation) follows the linear spectral mixture model (Adams et al., 1986), the temporal dynamics of the pixel spectrum was modeled by the changing fractions of these three components as follows:

$$R_m^t = f_{veg}^t R_{veg} + f_{soil}^t R_{soil} + f_{snow}^t R_{snow} \quad (7)$$

where $R_m^t R_m^t$ is the reflectance of the mixed pixel at time t, $R_{veg,}$ R_{soil} and $R_{snow} R_{veg}$, R_{soil} and R_{snow} are the reflectance values of vegetation, soil and snow respectively which are calculated by the spectra from the Aster Spectral Library and spectral response functions of MODIS, and f_{veg}^t, f_{soil}^t and f_{snow}^t f_{veg}^t, f_{soil}^t and f_{snow}^t are the fractions of the corresponding components at time t. The VI time series were then calculated based on the simulated reflectance on corresponding bands according to Eq. 6.

As Fig. 3 shows, in scenario 1 without snow cover, the snow coverage remains 0 from the beginning to the end of spring (210th day of year), the fraction of vegetation starts to increase on the 90th day. In scenario 2, the snowmelt begins on the 50th day and ends on the 100th day (snow coverage from 0.8 to 0.0). The vegetation coverage increases after snowmelt on the 130th day. In scenario 3, the snowmelt begins on the 70th day and ends on the 120th day. Vegetation coverage increases during the snowmelt period on the 100th day. For simplicity, all the changes are assumed to be linear. Here, we define GUD as the day when vegetation coverage fraction starts to increase. We also estimated the GUD from the VI time series from the inflection point of a piecewise linear model.

2.3. Measurements at the ecosystem phenology camera sites

Digital repeat photography from web camera has been used to monitor the vegetation phenology recently (e.g. Richardson et al., 2007; Sonnentag et al., 2012; Toomey et al., 2015). Compared with satellite-based remote sensing, digital cameras take images at much higher temporal frequencies, and obtain images that are free of contamination by clouds and not requiring correction for atmospheric effects. Digital photography provides opportunities for both direct visual assessment and quantitative analysis of the landscape dynamics.

We validated the performance of NDPI and other VIs at three ecosystem phenology camera sites (Table 1). US-UMB is located at the University of Michigan Biological Station. It mainly consists of deciduous forests with a long period of snow cover (Nave et al., 2011) (Fig. 4a). US-Ufp and US-Ufm are located at the University of Illinois Energy Farm. This area is spatially heterogeneous with a variety of agro-ecosystems. These two sites are spatially close and fall within one MODIS pixel. The digital cameras at the two sites monitor different land cover types. Imagery at US-Ufp shows a piece of restored prairie and US-Ufm shows a maize/soybean agro-ecosystem (Fig. 4b, c). Compared with US-UMB, there is rare snow fall in this area. The field of view of the cameras is smaller than a MODIS pixel.

The image data were downloaded from the PhenoCam Network http://phenocam.sr.unh.edu/webcam/. The digital cameras take images at high temporal frequencies (several images per day). We downloaded

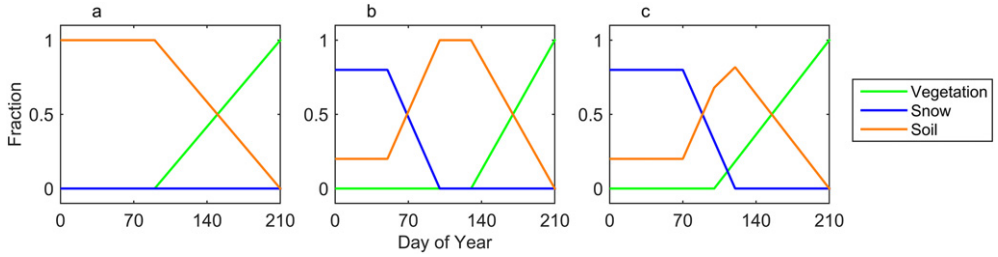

Fig. 3. Design of simulation experiment. a–c, temporal dynamics of the fraction of vegetation, snow and soil in scenario 1 (a), scenario 2 (b) and scenario 3 (c).

all the available images recorded at 10 a.m. to 2 p.m. during the period of 2009–2015. These images were firstly used to visually identify the dates with snow. To conduct further quantitative analysis, the red (R), green (G) and blue (B) digital numbers (DNs), which represent the relative brightness in these wavelengths, were extracted from the region of interest in the images (yellow polygons in Fig. 4). The green chromatic coordinate (GCC) was calculated for each image as:

$$GCC = \frac{G}{R+G+B} \tag{8}$$

where GCC is a camera-based index to monitor vegetation dynamics with many successful applications (Keenan et al., 2014; Sonnentag et al., 2012; Toomey et al., 2015). To further reduce the unexpected variability in GCC time series, we assigned the 90th percentile value from a 3-day moving window to the center date as proposed in Sonnentag et al. (2012). The images from Jan. to Apr. in 2013 at the US-UMB sites are missing, so that year was excluded from our analysis. We conducted the above processing of the PhenoCam data using the PhenocamGUI-W64 v1.1 application written in MATLAB (R2012b) obtained from http://phenocam.sr.unh.edu/webcam/tools/.

2.4. Measurements at the CO_2 flux sites

Gross primary production (GPP) values obtained from half-hourly EC CO_2 flux measurements at flux tower sites have been widely used to monitor the vegetation phenology (Balzarolo et al., 2016). We used these GPP values to validate the performance of NDPI at 10 flux tower sites including six deciduous broadleaf forest (DBF) sites, three agriculture cropland (CL) sites, and one grassland (GL) sites with a total of 116 site years from the AmeriFlux networks (http://ameriflux.ornl.gov/) and the FLUXNET (http://fluxnet.fluxdata.org/, Table 1). Besides, GPP data of site CN-Hab (37.6°N, 101.3°E) which is located on an alpine meadow in the northeast of Qinghai-Tibetan Plateau, China, was also obtained directly from the investigator of the site (Zhang and Tang, 2005). GPP was calculated by adding daytime net ecosystem production (NEP) to daytime ecosystem respiration (ER) which was obtained using the nighttime relationship between EC CO_2 fluxes and temperature (Moffat et al., 2007). The footprint of a flux tower is typically 100–2000 m which is approximately comparable with a pixel of satellite imagery (e.g. 500 m for MOD09A1, Baldocchi et al., 2001).

2.5. Remotely sensed data

The MODIS 500-m reflectance product (MOD09A1) was obtained from the Oak Ridge National Laboratory (https://daac.ornl.gov/MODIS/). It is 8-day composited by selecting the clearest conditions over the period. The product corrects for the effects of Rayleigh scattering, aerosols, gaseous absorption, thin cirrus clouds and the surface adjacency effect (Vermote and Vermeulen, 1999). We extracted the red, NIR and SWIR reflectance from a single pixel located at each camera site and flux tower site to calculate all the VI values (i.e. NDVI, NDII, PI and NDPI). The actual acquisition date of the MODIS product was used to construct the VI time series. The two camera sites, i.e. US-Ufp and US-Ufm, are located in the same MODIS pixel.

The MODIS land surface temperature (LST) product (MOD11A2) with a spatial resolution of 1-km and a time interval of 8-day was also downloaded from the Oak Ridge National Laboratory website. A linear interpolation method was used to estimate the missing values based on the temporal closest available values. The MOD11A2 dataset was used to remove the snow contamination in NDVI time series.

A three-point median-value filter was applied to the VI time series to remove outliers affected by cloud or poor atmospheric conditions (Zhang et al., 2006). For NDVI time series, we screened the snow contamination using the method proposed in Zhang et al. (2006), which was applied to produce the MODIS phenology products beforehand. The MODIS reflectance product provides a snow flag in its quality assurance file to indicate whether the data is snow free. Considering that the flag is not perfect, we further assigned pixels with LST values <5 °C as snow contaminated. We then replace these snow-influenced values with the temporal closest valid snow- free NDVI value.

Table 1
Detailed information about the PhenoCam and CO_2 flux tower sites. The bold words indicate the year of PhenoCam data.

Site ID	Site name	Latitude/longitude	IGBP[a,b] biome	Data year	Reference
CA_Oas	Saskatchewan–Western Boreal, Mature Aspen	53.6/−106.2	DBF	2000–2010 (11)	Barr et al., 2002
US_Oho	Oak Openings	41.6/−83.8	DBF	2004–2013 (10)	Noormets et al., 2008
US_MMS	Morgan Monroe State Forest	39.3/−86.4	DBF	2000–2013 (14)	Dragoni et al., 2011
US_UMB	Univ. of Mich. Biological Station	45.6/−84.7	DBF	2000–2013 (14)	Gough et al., 2013
US_WCr	Willow Creek	45.8/−90.1	DBF	2000–2006 (7)	Cook et al., 2004
US_Ha1	Harvard Forest	42.5/−72.2	DBF	2000–2012 (13) **2009–2015 (7)**	Urbanski et al., 2007
US-Ne1	Mead – irrigated continuous maize site	41.2/−96.5	CL	2001–2012 (12)	Verma et al., 2005
US-Ne2	Mead – irrigated maize-soybean rotation site	41.2/−96.5	CL	2001–2012 (12)	Verma et al., 2005
US-Bo1	Bondville	40.0/−88.3	CL	2000–2006 (7)	Dong et al., 2015
CN-Hab	Haibei Meadow	37.6/101.3	GL	2002–2012 (11)	Zhang and Tang, 2005
CA-Let	AB-Lethbridge Grassland	49.43–112.9	GL	2001–2005 (5)	Flanagan et al., 2002
US-Ufp	Uiefprairie	40.1/−88.2	GL	**2009–2015 (7)**	http://phenocam.sr.unh.edu/webcam/
US-Ufm	Uiefmaize	40.1/−88.2	CL	**2009–2015 (7)**	

[a] DBF is deciduous broadleaf forests; CL is croplands; GL is grassland.
[b] IGBP is the abbreviation of International Geosphere-Biosphere Programme.

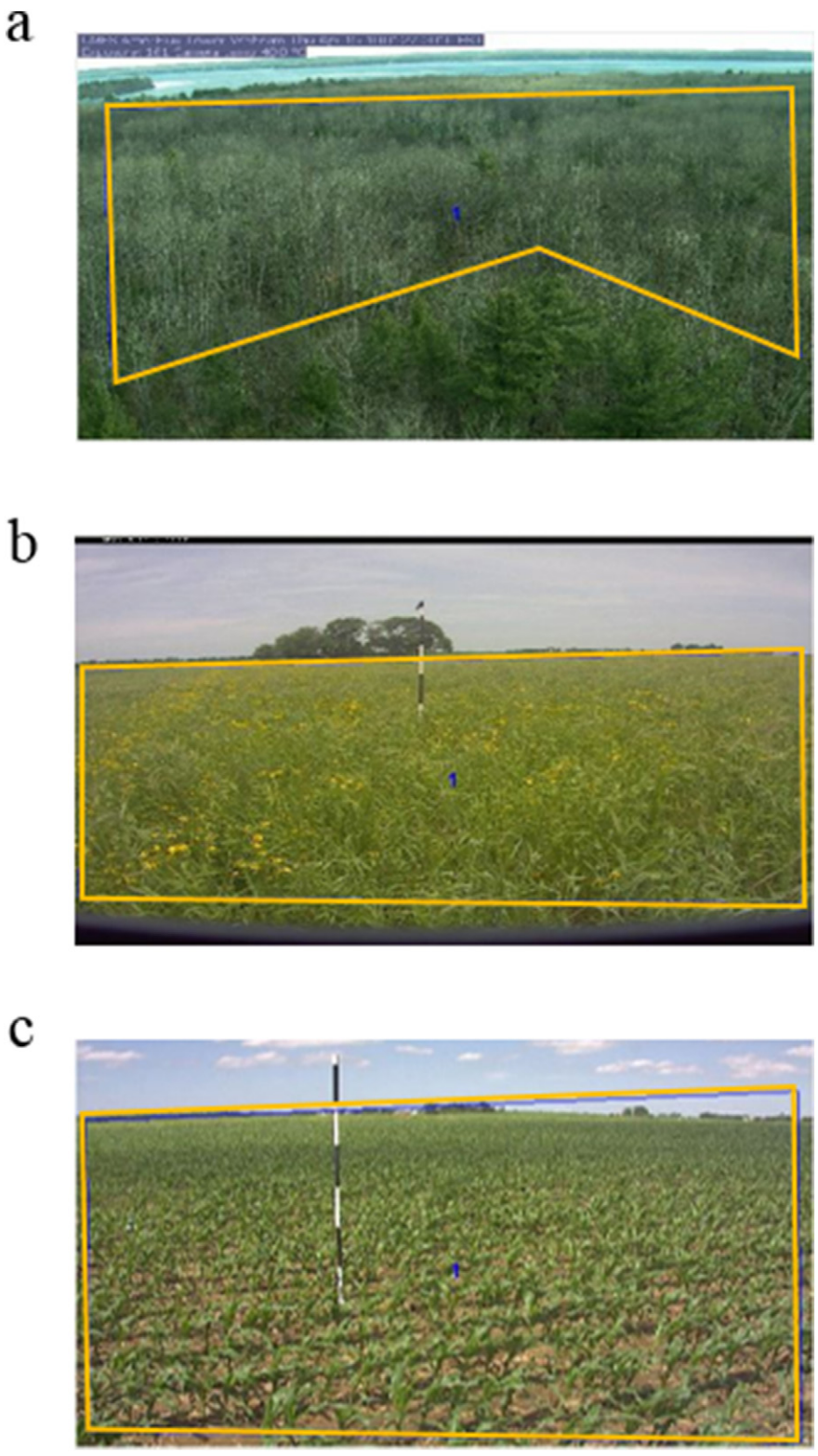

Fig. 4. Example images of the three camera sites. The yellow polygons show the regions of interest. a) US-UMB (45.6°N, 84.7°W); b) US-Ufp (40.1°N, 88.2°W); c) US-Ufm (40.1°N, 88.2°W).

To identify the GUD from the satellite/camera based VIs and daily GPP data at the camera and flux sites, we fit a sigmoid-shaped logistic function (Eq. 9) to each time series:

$$y(t) = \frac{c}{1 + e^{a+bt}} + d \tag{9}$$

where t is DOY and a, b, c and d are fitted parameters. The GUD is determined as the date of the first maximum rate of change of curvature (Zhang et al., 2003). The logistic fitting method has been widely used for the detection of GUD (e.g. Cao et al., 2015; Wang et al., 2015). In particular, it was adopted to produce the MODIS phenological product (MCD12Q2, Zhang et al., 2006). Hereafter, we did not estimate GUDs

from NDII data, because the seasonal profile of NDII is different from that of vegetation fraction, GCC, satellite based VIs or GPP. It cannot be described by a piecewise linear model (simulation experiment) or a sigmoid-shaped logistic function (camera and flux tower sites), which makes the GUD unable to be defined in the same way as other VIs. Previous studies usually used the threshold value method (Delbart et al., 2005; Dunn and de Beurs, 2011), but the threshold value is difficult to determine objectively since it is related to both the noise in remote sensing signals and vegetation growth (Delbart et al., 2005). We thus only analyzed the seasonal pattern of NDII qualitatively as Gonsamo et al. (2012).

3. Results

3.1. Validation by simulation test

We checked the VI time series for different scenarios. Fig. 5 and Fig. S1 show all the possible combinations of the spectral reflectance curves of 25 soil types, 4 snow types and 3 vegetation types. In scenario 1 without snow cover, each of NDVI, NDII and NDPI could well capture the variance of vegetation fraction (Fig. 5a). On average, the estimated GUD was only about 4.0 and 3.4 days earlier than the actual start of vegetation growth for NDVI and NDPI respectively (Fig. 5d). However, PI failed to capture the vegetation dynamics in the simplest scenario. When the vegetation fraction started to increase, PI remained zero, then followed with an unexpected sudden increase. By examining the mathematical form of PI, we found that PI is assigned to zero when NDII is less than zero to constrain the non-vegetation variance. Such a design causes PI to lose information from sparse vegetation since NDII could also be negative when vegetation coverage is low. This issue introduces large uncertainty in the detection of change in vegetation phenology, especially growth events in the spring when the vegetation is sparse. The GUD estimates from PI were dramatically overestimated with 26.1 days later than the true green-up day (Fig. 5d).

In scenario 2 with vegetation growth after snowmelt, NDVI increased after both snowmelt and green vegetation appearance, resulting in two distinct increases (Fig. 5b) and the GUD estimates were thus underestimated (i.e. 32.1 days earlier) (Fig. 5e). PI was insensitive to snowmelt, but was also insensitive to sparse vegetation resulting in overestimated GUDs (i.e. 17.5 days later). Both NDII and NDPI could distinguish the two processes well in this case. NDII decreased during snowmelt and increased during vegetation growth while NDPI remained stable during snowmelt and started to increase as soon as the fraction of vegetation began to increase. The GUD estimates from NDPI were only 2.4 days earlier than the simulated green-up (Fig. 5e).

In scenario 3 with vegetation growth during the snowmelt period, NDVI and PI had the same issues as in scenario 2 and/or scenario 1. The GUD estimates based on NDVI and PI were 21.9 days earlier and 24.2 days later than the simulated green-up (Fig. 5d and e). NDII also failed in this situation. The expected increase in NDII caused by vegetation growth was masked by snowmelt (Fig. 5c). NDPI, however, still performed well. The estimated GUDs were only 0.4 days earlier than the simulated GUD (Fig. 5f).

3.2. Validation at the ecosystem phenology camera sites

Fig. 6 shows the seasonal profiles of VIs during 2009–2015. Table 2 gives the detected GUD values by VIs and the comparison with reference GUD values detected by GCC time series during the same period. US-UMBS is a BDF site with long periods of snow cover, from December of the previous year to April. As expected, the NDVI remained low and unstable during winter and early spring when there was snow cover. It started to increase at the end of the snow covered period. In this case, the initiation of vegetation growth immediately followed snowmelt, resulting in a continuous increase in NDVI. Without removing the influence of snow, the NDVI time series failed to monitor the vegetation phenology. The estimated GUD was more than one month earlier than the GCC-based GUD (not shown here). After removing the snow contamination, the NDVI-based estimates were close to the GCC-based estimates and the bias was improved to about −3.7 days (Table 2). The NDII of snow was comparable with that of vegetated landscape. In

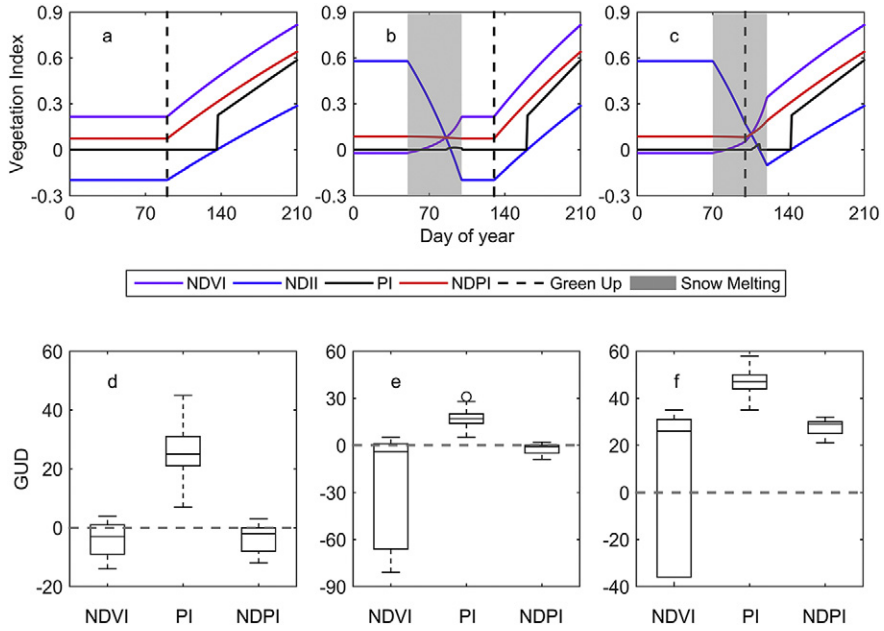

Fig. 5. Results of simulation experiment. a–c, temporal evolution of the vegetation indices (VIs) in scenario 1 (a), scenario 2 (b) and scenario 3 (c). The reflectance spectrum used in a–c for Eq. (7) is the average of spectrum types listed in Table S1. The three spectrum curves are shown in Fig. 1. The dashed line shows the date when the fraction of vegetation starts to increase and the gray shadow shows the period of snowmelt. d–f, the boxplot of the difference between the green-up date (GUD) estimated from NDVI, PI, NDPI and the start of the increase of vegetation fraction in scenario 1 (d), scenario 2 (e) and scenario 3 (f). All the possible combinations of the 25 soil types, 4 snow types and 3 vegetation types are involved in the boxplot (d–f).

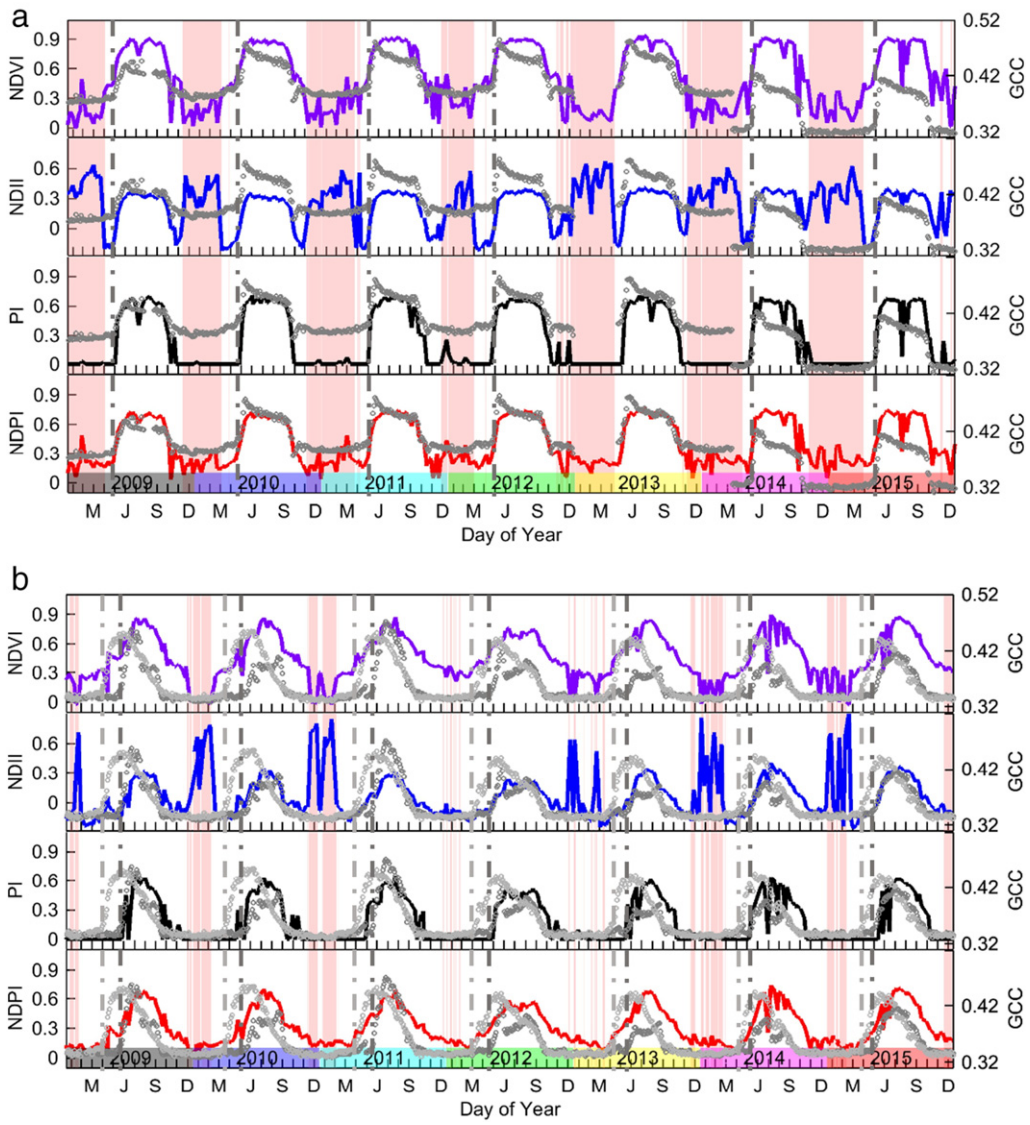

Fig. 6. Example time series of NDVI, NDII, PI, NDPI and GCC for the PhenoCam sites, the US-UMB site (a) and the US-Ufp and US-Ufm sites (b). The pink shadow is the snow covered period. The colored lines show the satellite based VI time series and the gray circles are the GCC values. The gray dash lines indicate the GCC based GUD. In panel b, the dark circle (dash line) is site US-Ufm and the light circle (dash line) is the site US-Ufp. The snow coverage information during spring in 2003 at US-UMB site was derived from images from another camera at the same site.

some years like 2014–2015, the vegetated period becomes indistinguishable from the snow-covered period. PI could well constrain the non-vegetation variance. The expected time period when PI is insensitive to sparse vegetation was not distinct in this case, although close examination of photos indicated that the increase of PI in the spring was a little later than GCC in some years such as 2010 (Fig. 6a and Table 2). The reason is probably that the vegetation is dense and the appearance of foliage is rapid in the DBF site. The 8-day composition NDVI data may easily miss this short period when the vegetation is sparse. The estimated GUD from PI was close to that of camera images. The bias was only 3.7 days, i.e. 3.7 days later than the reference on average (Table 2). We then checked the performance of NDPI. Snowmelt did not cause any systematic shift in NDPI. The variability of NDPI in winter was lower than NDVI but higher than PI. However, this variability did not influence the detection of the GUD. The GUD estimated from NDPI was only 2.0 days earlier than the estimates from GCC which was both better than PI or the snow removed NDVI.

The US-Ufp and US-Ufm sites are located in the same MODIS pixel, where snow fall is rare and intermittent (see pink shadows in Fig. 6b). The VI time series were much smoother than those for the US-UMBS site. The effect of snow on NDVI and NDII was consistent with the previous analysis. Interestingly, Fig. 6b shows the large difference between NDPI and PI. Both VIs were insensitive to snow but the increase of NDPI was much earlier than PI. This early increase of NDPI should not be attributed to snowmelt because no snow cover during the periods was shown in Fig. 6b. By comparing the increase in NDVI and NDII, it was highly likely to be caused by vegetation growth that was confirmed by checking the photos from the two cameras. It was found that the increase of NDPI was as early as the GCC time series for the US-Ufp site (restored prairie) while the increase of GCC for the US-Ufm (maize/soybean agro-ecosystem) was much later (Table 2). We cannot directly compare the GCC-based GUDs with the estimates from NDPI and PI for this case because of the high heterogeneity of vegetation in this MODIS pixel. However, we can confirm that when a fraction of the vegetation in the MODIS pixel, i.e. the prairie of the US-Ufp site, begins to grow, NDPI could capture these dynamics while PI was unresponsive because PI is insensitive to sparse vegetation. This was consistent with the results in the simulation experiment.

Table 2
GUD estimates based on VI (NDVI, PI, NDPI) time series and the green chromatic coordinate (GCC) at the three camera sites. The three columns on the right hand side show the difference between the satellite-based estimates and the camera-based estimates.

		NDVI	PI	NDPI	GCC	NDVI-GCC	PI-GCC	NDPI-GCC
US_UMB	2009	130	141	130	129	1	12	1
	2010	120	133	121	124	−4	9	−3
	2011	130	137	134	135	−5	2	−1
	2012	127	128	127	131	−4	−3	−4
	2013	/	/	/	/	/	/	/
	2014	142	142	145	144	−2	−2	1
	2015	126	138	129	134	−8	4	−5
	Mean	129.14	136.71	131.00	133.00	−3.67	3.67	−1.83
US_Ufm	2009	113	171	121	156	−43	15	−35
	2010	104	144	109	138	−34	6	−29
	2011	90	124	95	151	−61	−27	−56
	2012	82	136	93	128	−46	8	−35
	2013	98	156	113	150	−52	6	−37
	2014	130	137	132	144	−14	−7	−12
	2015	102	147	110	131	−29	16	−21
	Mean	102.71	145.00	110.43	142.57	−39.86	2.43	−32.14
US_Ufp	2009	113	171	121	104	9	67	17
	2010	104	144	109	91	13	53	18
	2011	89	124	95	101	−12	23	−6
	2012	82	136	93	73	9	63	20
	2013	97	157	113	109	−12	48	4
	2014	130	137	132	111	19	26	21
	2015	102	147	110	101	1	46	9
	Mean	102.43	145.14	110.43	98.57	3.86	46.57	11.86

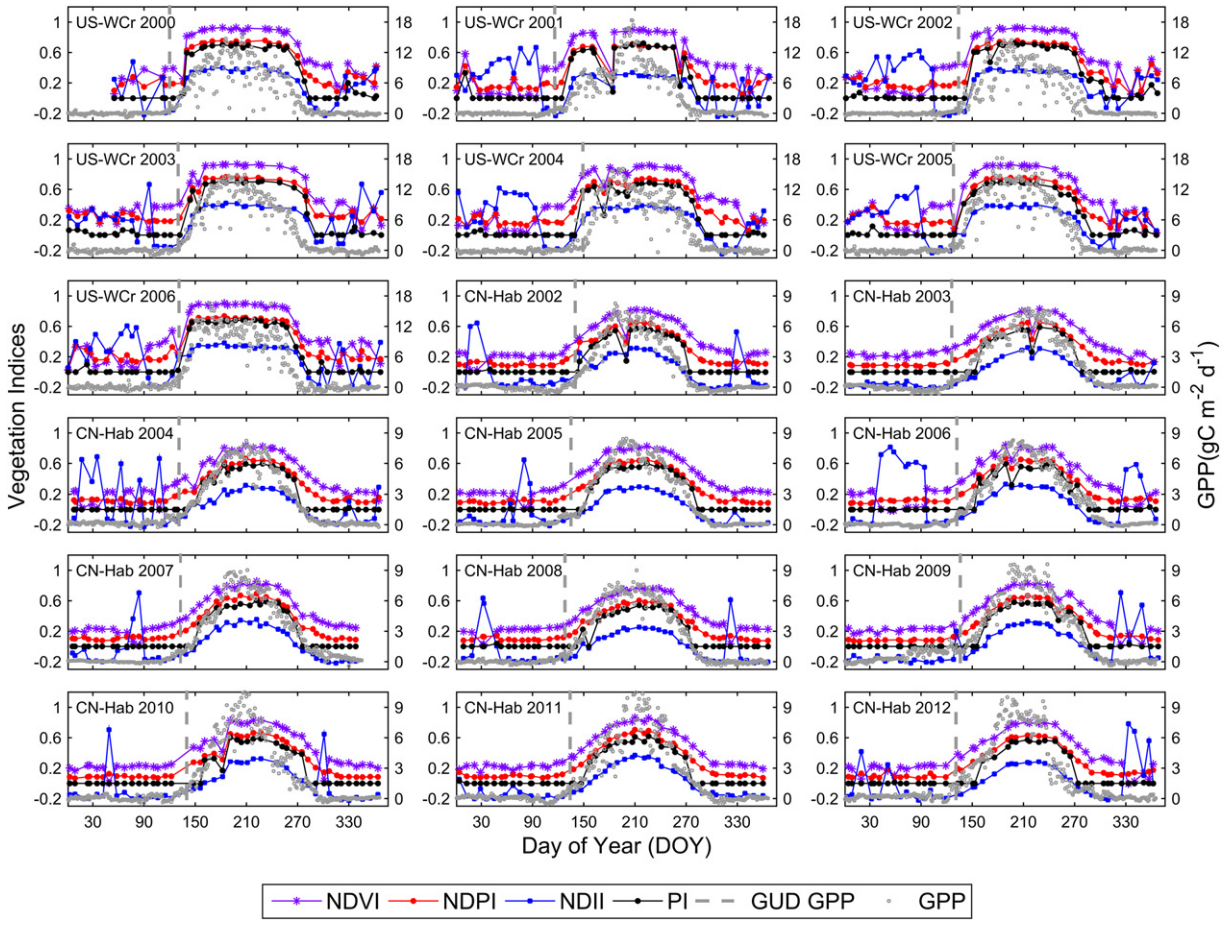

Fig. 7. Example time series of NDVI, NDII, PI, NDPI and GPP for a forest site US_WCr and a grassland site CN-Hab.

3.3. Validation at the CO_2 flux sites

We compared the VI time series with the temporal dynamics of GPP (Fig. 7, Figs. S2 and S3). In general, the results confirmed the observed behavior of the VIs at the camera sites and simulation experiments. In the BDF sites, the most common pattern of NDVI dynamic in spring was the stair-like shape (e.g. US-WCr 2001 and 2002 in Fig. 7, CA-Oas 2002 and US-UMB 2002 in Fig. S2) indicating a period with bare surface between the end of snowmelt and the beginning of vegetation growth. A continuous increase in NDVI started with snowmelt and closely followed with vegetation growth was also observed in some cases (e.g. CA-Oas 2003 in Fig. S2). Both PI and NDPI dealt with the two situations well at most site years. However, at most study years of US-Ha1 (e.g. 2003 and 2004 in Fig. S2), PI increased with a decrease of NDII in the spring when GPP and NDPI remained stable, implying a better performance of NDPI in these cases. The pattern of NDII was as expected. Snowmelt caused a decrease in NDII and vegetation growth caused an increase in NDII. NDII seems more sensitive to snow than vegetation for some sites (e.g. US-UMB in Fig. S2), the vegetation caused variability in NDII is weaker than that caused by snow which could introduce considerable uncertainty in phenology detection.

At CL/GL sites, snow fall is rare. When there was no snow, the seasonal profiles of NDVI and NDPI were similar (e.g. CN-Hab 2003 and 2011 in Fig. 7). At other site years, intermittent drops were observed in the NDVI time series while the NDPI curves were smooth, demonstrating that NDPI was insensitive to variance in snow cover (e.g. CN-Hab 2004 in Fig. 7 and US-Ne2 2002 in Fig. S3). PI was free of snow contamination as well. The increase of PI in the spring lagged the increase of GPP because PI was insensitive to sparse vegetation (e.g. CN-Hab 2006 in Fig. 7 and US-Ne1 2005 in Fig. S3). At the CA-Let site, PI remained zero throughout the whole year for some site years because of the sparse vegetation (e.g CA-Let 2001 in Fig. S3). The pattern of NDII was similar to that of NDVI but with intermittent peaks (e.g. CN-Hab 2006 in Fig. 7 and US-Bo1 2003 in Fig. S3). At the CA-Let site, the response of NDII to vegetation was too weak to monitor the vegetation dynamics.

Quantitatively, we compared GUD values derived from the VI time series to GUD values derived from the GPP data. Here, we used snow-removed NDVI, raw NDPI and raw PI to detect the GUD (see methodology and data). We did not estimate the GUD in CA-Let using PI because PI failed to extract the GUD at this site. Fig. 8 shows the scatterplots of GUD values estimated using VIs vs. GUD values estimated using GPP. Table 3 shows the corresponding measures of the agreement between them. The overall results confirmed the aforementioned qualitative analysis, implying that NDPI based GUD detection was more comparable with GPP than NDVI or PI. At the DBF sites, the performance of PI is poor for US-Ha1 site (Fig. 8). Results of other sites indicate that the three VIs were equally effective. The best performance of RMSE (7.68), Bias (1.96) and Correlation Coefficient (R, 0.87) were observed in NDPI, NDPI, and PI respectively. For the CL/GL sites, the performance of NDPI overwhelmingly exceeded that of snow removed NDVI and PI. The RMSE, Bias and R were 7.85, 4.17 and 0.86 for NDPI. The performance remained very similar after adding the CA-Let site, with respective values of 8.08, 3.15, and 0.87. The estimated start of PI increase was almost 2 weeks later than the GUD derived from GPP, which was close to results obtained in previous studies (e.g. Gonsamo et al., 2012). During the above analysis, site year US-Bo1 2002 was also excluded because the estimated GUD from GPP was dramatically different with those from VIs (Fig. 8). We checked the raw VIs and GDD data at this site year and found that the curve fitting based on GPP data was unreliable (not shown here).

By the definition of NDPI, α used in this study (0.74) may be not universally applicable although we demonstrated its validity for different plant functional types, including boreal and temporal deciduous forest (e.g. CA-Oas, US-MMS), cropland (e.g. US-Ne1), semiarid grassland (e.g. CA-Let), and alpine meadow (e.g. CN-Hab). We thus tested the sensitivity of the GUD estimates to α. NDPI time series with α ranging from 0.5 to 0.9 (0.01 step) were calculated for each flux tower site years. GUD was then derived from these NDPI time series. On average, 1% increase in.

α caused about 0.4 day advance in GUD estimates (Fig. 9). Fig. 10 shows the degree of the agreement between the GUD estimated using NDPI and GPP. The results indicate that (1) the performance of NDPI was acceptable with α ranging from about 0.6 to 0.8; (2) the performance of NDPI could be improved when α was optimized at local sites, although it already outperformed PI and the snow-removed NDVI when a common value of 0.74 was used. Readers should be aware that when α was <0.6, the bias, RMSE, and Correlation Coefficient still implied a good performance of NDPI. However, we found that with decreasing α, the seasonal profile of NDPI approached to that of NDII which was no longer a sigmoidal shape. It introduced large uncertainties in the curve fitting when the initial values of the parameters were not suitable (*nlinfit* function in Matlab-R2012b).

4. Discussion and summary

Vegetative spring phenology of temperate and boreal ecosystems is sensitive to climate change. However, the green-up date (GUD; an important indicator of spring phenology) detected by satellite based VIs, which include but are not limited to NDVI, is still largely sensitive to artifacts associated with snowmelt (Delbart et al., 2005; Gonsamo et al., 2012; Huete et al., 2002; Shabanov et al., 2002; White et al., 2005). This is especially evident in a recent study, in which the derived GUD (referred to as the start of growing season in the literature) using the NDVI approach showed large variation across 10 different methods (White et al., 2009). In addition, the derived GUD was found to be related to not only the vegetation phenological stages but also the cryospheric/hydrologic metrics. Consequently, minimizing the snowmelt effect on satellite-detected spring phenology has been a central focus in remote sensing-based phenology studies for decades (White et al., 2005).

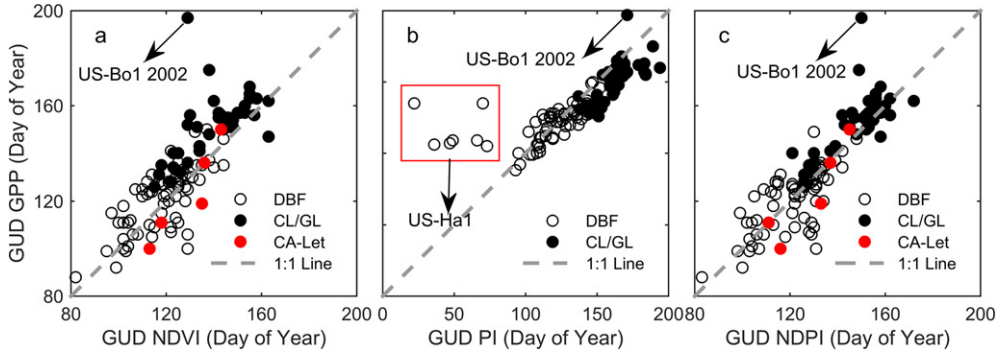

Fig. 8. Scatterplots of green-up date (GUD) as estimated from NDVI (a), PI (b), NDPI (c) against GPP for deciduous broadleaf forest (DBF), cropland (CL) and grassland (GL). The CA-Let site was excluded in (b) because PI failed to extract the GUD at this site.

Table 3
Quantitative measures of the agreement between the green-up date (GUD) estimated from NDVI, PI, NDPI and eddy-covariance-derived gross primary production (GPP) for DBF (deciduous broadleaf forests) and CL (cropland)/GL (glassland) vegetation types. The Root Mean Error (RMSE), Bias and Spearman's Correlation Coefficient (R) are shown. The CA-Let and US-Ha1 sites were excluded in the calculating except for the results in the bracket.

	NDVI			PI			NDPI		
	DBF	CL/GL	ALL	DBF	CL/GL	ALL	DBF	CL/GL	ALL
RMSE	9.03 (9.90)	13.04 (12.76)	10.91 (11.14)	7.98	15.94	12.00	**7.68** (9.68)	**7.85** (8.08)	**7.75** (9.07)
Bias	5.30 (2.51)	10.1 (8.39)	7.34 (4.86)	−3.07	−13.46	−7.46	**1.96** (−0.54)	**4.17** (3.15)	**2.90** (0.94)
R	0.85 (0.74)	0.80 (0.78)	0.90 (0.85)	**0.87**	0.79	0.93	0.86 (0.74)	**0.86** (0.87)	**0.93** (0.88)

Here, we developed a new vegetation index, i.e., Normalized Difference Phenology Index (NDPI), aiming to improve spring phenology monitoring using satellite techniques. Readers should be aware that NDPI is not designed to track temporal trajectories of vegetation dynamics better; instead, it is designed to be resistant to the snowmelt effect, by best contrasting vegetation signal from the backgrounds (e.g. snow and soil) while minimizing the difference between different background components. NDPI employs the red, near-infrared, and short wave infrared bands, which reflect the three major biochemical interactions between solar radiation and green leaves, including the visual light (red band) absorbed by chemical pigments (i.e. chlorophyll), the multiple scattering of NIR within leaf internal structure, and the absorption of shortwave infrared by leaf water content. In addition, it utilizes a similar 'normalized difference' mathematical form as NDVI which is intended to reduce many forms of multiplicative noise present in multiple bands (Huete et al., 2002).

In previous researches for GUD detection based on NDVI or EVI data, an additional step is usually needed to screen snow. However, these snow screening methods are not perfect and there is a lack of universally acceptable method, resulting in incomparable results from different literatures in some sense. When using NDPI, it wouldn't need such an additional step. Our analysis using a mathematical simulation test, digital repeated camera observations and EC flux tower observations further indicate that the GUD estimated from NDPI is more accurate than those based on NDVI even if a snow screening method was applied to the NDVI time series (Figs. 3, 5 and 6). Therefore, NDPI is advantageous relative to NDVI in motoring vegetative spring phenology. Compared to other VIs such as NDII and PI, NDPI is more sensitive to vegetation growth (Fig. 6 and Fig. S2) and can more accurately detect the GUD even when vegetative growth occurs the same time as snowmelt (Fig. 3). Note that PI failed to capture the early green-up of the restored prairie in US-Ufp/US-Ufm sites because it is insensitive to sparse vegetation. However, it successfully detected the late green-up of the maize/soybean agro-ecosystem, suggesting that a combined use of NDPI, PI or other VIs may help identify the multiple green-up dates in heterogeneous regions with multiple vegetation communities. This argument awaits further examination in future works. Since our study spans the sites of a wide latitudinal range (37.6°N-53.6°N) and covers various vegetation types (deciduous forest, cropland, semiarid grassland and alpine meadow), our results thus suggest the newly developed NDPI has the potential to improve vegetative spring phenology monitoring over large-scale in snow covered regions.

NDPI also has limitations. Firstly, α, an important coefficient of NDPI (Eq. 6), might not be universally applicable. Here, by using the data across a wide range of vegetation types, we observe that when $\alpha = 0.74$, satellite-detected spring phenology is in good agreement with ground observations. However, this value of α may not be universally applicable, and we still need data from more site-year to better understand and constrain it in future analyses. Secondly, NDPI might not be applicable to evergreen forests (e.g. temperate pine forests). This is because NDPI is designed for the ecosystems which are composited by

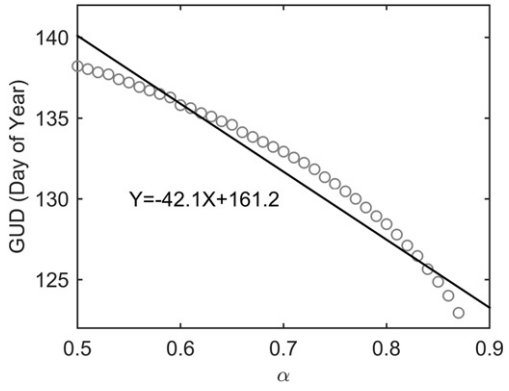

Fig. 9. Green-up date (GUD) estimated from NDPI with α ranging from 0.5 to 0.9. Each dot is the average of the 59 site years. The site CA-Let, US-Ha1 and US-Bo1 2002 were excluded. Linear regression is shown as the line and equation.

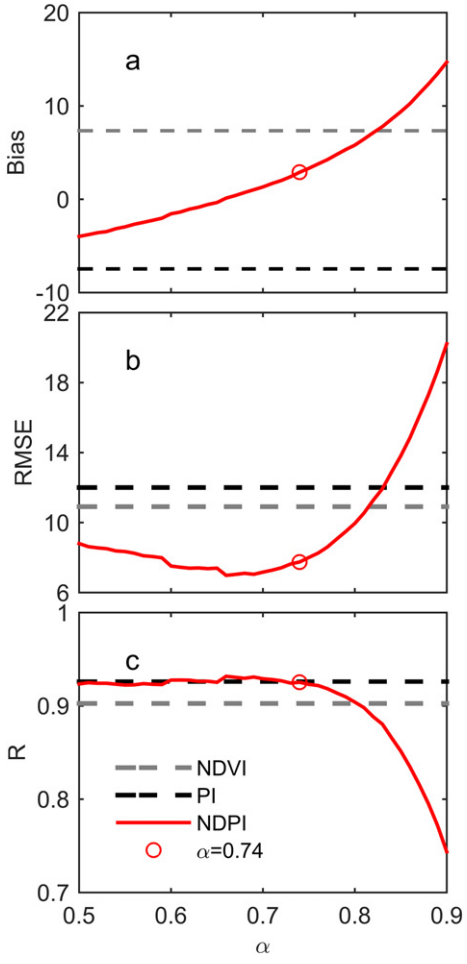

Fig. 10. The Root Mean Error (RMSE), Bias and Spearman's Correlation Coefficient (R) between the green-up date (GUD) estimated from NDPI with α ranging from 0.5 to 0.9 and GPP. The site CA-Let, US-Ha1 and US-Bo1 2002 were excluded. The purple and black dashed lines show the results for NDVI and PI, respectively.

litter, soil and snow in non-growing season. As such, NDPI might not be optimal for evergreen forests in which the green foliar are also present in the non-growing season. For other biomes which were not included in this analysis such as tundra ecosystems, we highlight that NDPI should work well but whether the α value in current study is still appropriate is unknown. Thirdly, NDPI is designed for spring phenology, it is not necessary a better indicator for detecting fall phenology. Finally, NDPI is not expected to track temporal trajectories of vegetation dynamics better. The profiles of NDVI and NDPI are similar during the growing season indicating an equal performance of the two VIs.

Snowmelt effect is a long standing issue in vegetative spring phenology monitoring using satellite-based VIs. Promising results here suggest that NDPI is a reliable approach for phenology monitoring because it is more resistant to snowmelt effect than any other existing VIs. We therefore recommend the community to utilize NDPI to monitor vegetation spring phenology as well as to assess whether the spring phenology derived by using this approach can better constrain the phenological parameterization of earth system models as well as to improve the understanding of climate impacts on spring phenology.

Acknowledgements

This study is supported by 1) the Fund for Creative Research Groups of National Natural Science Foundation of China (No. 41321001), 2) the project of "Early detection and prediction of climate warming based on the long-term monitoring of fragile ecosystems in the East Asia" funded by the Ministry of Environment, Japan (MOJ-Kan-1351). We thank Andrew Richardson and members of the PhenoCam team for making PhenoCam imagery freely available, and the many collaborators, including site PIs and technicians, without whom the PhenoCam project would not be possible. The development of PhenoCam has been supported by the Northeastern States Research Cooperative, NSF's Macrosystems Biology Program (award EF-1065029), DOE's Regional and Global Climate Modeling Program (award DE-SC0016011), and the US National Park Service Inventory and Monitoring Program and the USA National Phenology Network (grant number G10AP00129 from the United States Geological Survey). We also thank for FLUXNET and AmeriFlux to provide the flux data. The funding for AmeriFlux data resources was provided by the U.S. Department of Energy's Office of Science.

Appendix A. Supplementary data

Supplementary data to this article can be found online at http://dx.doi.org/10.1016/j.rse.2017.04.031.

References

Adams, J.B., Smith, M.O., Johnson, P.E., 1986. Spectral mixture modeling: a new analysis of rock and soil types at the Viking Lander 1 site. J. Geophys. Res. Solid Earth 91, 8098–8112.

Asrar, G., Fuchs, M., Kanemasu, E., Hatfield, J., 1984. Estimating absorbed photosynthetic radiation and leaf area index from spectral reflectance in wheat. Agron. J. 76, 300–306.

Baldocchi, D., Falge, E., Gu, L., Olson, R., Hollinger, D., Running, S., Anthoni, P., Bernhofer, C., Davis, K., Evans, R., 2001. FLUXNET: a new tool to study the temporal and spatial variability of ecosystem-scale carbon dioxide, water vapor, and energy flux densities. Bull. Am. Meteorol. Soc. 82, 2415–2434.

Baldridge, A., Hook, S., Grove, C., Rivera, G., 2009. The ASTER spectral library version 2.0. Remote Sens. Environ. 113, 711–715.

Balzarolo, M., Vicca, S., Nguy-Robertson, A., Bonal, D., Elbers, J., Fu, Y., Grünwald, T., Horemans, J., Papale, D., Peñuelas, J., 2016. Matching the phenology of Net Ecosystem Exchange and vegetation indices estimated with MODIS and FLUXNET in-situ observations. Remote Sens. Environ. 174, 290–300.

Barr, A., Griffis, T., Black, T., Lee, X., Staebler, R., Fuentes, J., Chen, Z., Morgenstern, K., 2002. Comparing the carbon budgets of boreal and temperate deciduous forest stands. Can. J. For. Res. 32, 813–822.

Beck, P.S., Atzberger, C., Høgda, K.A., Johansen, B., Skidmore, A.K., 2006. Improved monitoring of vegetation dynamics at very high latitudes: a new method using MODIS NDVI. Remote Sens. Environ. 100, 321–334.

Buitenwerf, R., Rose, L., Higgins, S.I., 2015. Three decades of multi-dimensional change in global leaf phenology. Nat. Clim. Chang. 5 (4), 364–368.

Cao, R., Chen, J., Shen, M., Tang, Y., 2015. An improved logistic method for detecting spring vegetation phenology in grasslands from MODIS EVI time-series data. Agric. For. Meteorol. 200, 9–20.

Cook, B.D., Davis, K.J., Wang, W., Desai, A., Berger, B.W., Teclaw, R.M., Martin, J.G., Bolstad, P.V., Bakwin, P.S., Yi, C., 2004. Carbon exchange and venting anomalies in an upland deciduous forest in northern Wisconsin, USA. Agric. For. Meteorol. 126, 271–295.

Delbart, N., Kergoat, L., Le Toan, T., Lhermitte, J., Picard, G., 2005. Determination of phenological dates in boreal regions using normalized difference water index. Remote Sens. Environ. 97, 26–38.

Delbart, N., Le Toan, T., Kergoat, L., Fedotova, V., 2006. Remote sensing of spring phenology in boreal regions: a free of snow-effect method using NOAA-AVHRR and SPOT-VGT data (1982–2004). Remote Sens. Environ. 101, 52–62.

Dong, J., Xiao, X., Wagle, P., Zhang, G., Zhou, Y., Jin, C., Torn, M.S., Meyers, T.P., Suyker, A.E., Wang, J., 2015. Comparison of four EVI-based models for estimating gross primary production of maize and soybean croplands and tallgrass prairie under severe drought. Remote Sens. Environ. 162, 154–168.

Dragoni, D., Schmid, H.P., Wayson, C.A., Potter, H., Grimmond, C.S.B., Randolph, J.C., 2011. Evidence of increased net ecosystem productivity associated with a longer vegetated season in a deciduous forest in south-central Indiana, USA. Glob. Chang. Biol. 17, 886–897.

Dunn, A.H., de Beurs, K.M., 2011. Land surface phenology of North American mountain environments using moderate resolution imaging spectroradiometer data. Remote Sens. Environ. 115, 1220–1233.

Fensholt, R., Sandholt, I., 2003. Derivation of a shortwave infrared water stress index from MODIS near-and shortwave infrared data in a semiarid environment. Remote Sens. Environ. 87, 111–121.

Flanagan, L.B., Wever, L.A., Carlson, P.J., 2002. Seasonal and interannual variation in carbon dioxide exchange and carbon balance in a northern temperate grassland. Glob. Chang. Biol. 8, 599–615.

Fu, Y.H., Liu, Y., De Boeck, H.J., Menzel, A., Nijs, I., Peaucelle, M., Peñuelas, J., Piao, S., Janssens, I.A., 2016. Three times greater weight of daytime than of night-time temperature on leaf unfolding phenology in temperate trees. New Phytol. 212 (3), 590–597.

Gao, B.-C., 1996. NDWI—a normalized difference water index for remote sensing of vegetation liquid water from space. Remote Sens. Environ. 58, 257–266.

Gonsamo, A., Chen, J.M., Price, D.T., Kurz, W.A., Wu, C., 2012. Land surface phenology from optical satellite measurement and CO_2 eddy covariance technique. J. Geophys. Res. Biogeosci. 2005–2012, 117.

Gough, C.M., Hardiman, B.S., Nave, L.E., Bohrer, G., Maurer, K.D., Vogel, C.S., Nadelhoffer, K.J., Curtis, P.S., 2013. Sustained carbon uptake and storage following moderate disturbance in a Great Lakes forest. Ecological Applications A Publication of the Ecological Society of America 23, 1202–1215.

Hardisky, M., Klemas, V., Smart, R.M., 1983. The influence of soil salinity, growth form, and leaf moisture on the spectral radiance of *Spartina alterniflora* canopies. Photogramm. Eng. Remote. Sens. 49, 77–83.

Huete, A., Didan, K., Miura, T., Rodriguez, E.P., Gao, X., Ferreira, L.G., 2002. Overview of the radiometric and biophysical performance of the MODIS vegetation indices. Remote Sens. Environ. 83, 195–213.

Karlsen, S.R., Elvebakk, A., Høgda, K.A., Grydeland, T., 2014. Spatial and temporal variability in the onset of the growing season on Svalbard, Arctic Norway—measured by MODIS-NDVI Satellite Data. Remote Sens. 6, 8088–8106.

Keenan, T., Darby, B., Felts, E., Sonnentag, O., Friedl, M., Hufkens, K., O'Keefe, J., Klosterman, S., Munger, J.W., Toomey, M., 2014. Tracking forest phenology and seasonal physiology using digital repeat photography: a critical assessment. Ecol. Appl. 24, 1478–1489.

Menzel, A., Fabian, P., 1999. Growing season extended in Europe. Nature 397, 659.

Moffat, A.M., Papale, D., Reichstein, M., Hollinger, D.Y., Richardson, A.D., Barr, A.G., Beckstein, C., Braswell, B.H., Churkina, G., Desai, A.R., 2007. Comprehensive comparison of gap-filling techniques for eddy covariance net carbon fluxes. Agric. For. Meteorol. 147, 209–232.

Myneni, R.B., Keeling, C., Tucker, C., Asrar, G., Nemani, R., 1997. Increased plant growth in the northern high latitudes from 1981 to 1991. Nature 386, 698–702.

Nagler, P., Daughtry, C., Goward, S., 2000. Plant litter and soil reflectance. Remote Sens. Environ. 71, 207–215.

Nave, L., Gough, C., Maurer, K., Bohrer, G., Hardiman, B., Le Moine, J., Munoz, A., Nadelhoffer, K., Sparks, J., Strahm, B., 2011. Disturbance and the resilience of coupled carbon and nitrogen cycling in a north temperate forest. J. Geophys. Res. Biogeosci. 2005–2012, 116.

Noormets, A., McNulty, S.G., DeForest, J.L., Sun, G., Li, Q., Chen, J., 2008. Drought during canopy development has lasting effect on annual carbon balance in a deciduous temperate forest. New Phytol. 179, 818–828.

Parmesan, C., Yohe, G., 2003. A globally coherent fingerprint of climate change impacts across natural systems. Nature 421, 37–42.

Peckham, S.D., Ahl, D.E., Serbin, S.P., Gower, S.T., 2008. Fire-induced changes in green-up and leaf maturity of the Canadian boreal forest. Remote Sens. Environ. 112, 3594–3603.

Pettorelli, N., Vik, J.O., Mysterud, A., Gaillard, J.-M., Tucker, C.J., Stenseth, N.C., 2005. Using the satellite-derived NDVI to assess ecological responses to environmental change. Trends Ecol. Evol. 20, 503–510.

Richardson, A.D., Jenkins, J.P., Braswell, B.H., Hollinger, D.Y., Ollinger, S.V., Smith, M.-L., 2007. Use of digital webcam images to track spring green-up in a deciduous broadleaf forest. Oecologia 152, 323–334.

Richardson, A.D., Hollinger, D.Y., Dail, D.B., Lee, J.T., Munger, J.W., O'keefe, J., 2009. Influence of spring phenology on seasonal and annual carbon balance in two contrasting New England forests. Tree Physiol. 29, 321–331.

Richardson, A.D., Black, T.A., Ciais, P., Delbart, N., Friedl, M.A., Gobron, N., Hollinger, D.Y., Kutsch, W.L., Longdoz, B., Luyssaert, S., 2010. Influence of spring and autumn phenological transitions on forest ecosystem productivity. Philosophical Transactions of the Royal Society B: Biological Sciences 365, 3227–3246.
Shabanov, N.V., Zhou, L., Knyazikhin, Y., Myneni, R.B., Tucker, C.J., 2002. Analysis of interannual changes in northern vegetation activity observed in AVHRR data from 1981 to 1994. IEEE Trans. Geosci. Remote Sens. 40, 115–130.
Shen, M., Sun, Z., Wang, S., Zhang, G., Kong, W., Chen, A., Piao, S., 2013. No evidence of continuously advanced green-up dates in the Tibetan Plateau over the last decade. Proc. Natl. Acad. Sci. 110, E2329.
Sonnentag, O., Hufkens, K., Teshera-Sterne, C., Young, A.M., Friedl, M., Braswell, B.H., Milliman, T., O'Keefe, J., Richardson, A.D., 2012. Digital repeat photography for phenological research in forest ecosystems. Agric. For. Meteorol. 152, 159–177.
Thompson, J.A., Paull, D.J., Lees, B.G., 2015. Using phase-spaces to characterize land surface phenology in a seasonally snow-covered landscape. Remote Sens. Environ. 166, 178–190.
Toomey, M., Friedl, M.A., Frolking, S., Hufkens, K., Klosterman, S., Sonnentag, O., Baldocchi, D.D., Bernacchi, C.J., Biraud, S.C., Bohrer, G., 2015. Greenness indices from digital cameras predict the timing and seasonal dynamics of canopy-scale photosynthesis. Ecol. Appl. 25, 99–115.
Urbanski, S., Barford, C., Wofsy, S., Kucharik, C., Pyle, E., Budney, J., McKain, K., Fitzjarrald, D., Czikowsky, M., Munger, J., 2007. Factors controlling CO2 exchange on timescales from hourly to decadal at Harvard Forest. J. Geophys. Res. Biogeosci. 2005–2012, 112.
Verma, S.B., Dobermann, A., Cassman, K.G., Walters, D.T., Knops, J.M., Arkebauer, T.J., Suyker, A.E., Burba, G.G., Amos, B., Yang, H., 2005. Annual carbon dioxide exchange in irrigated and rainfed maize-based agroecosystems. Agric. For. Meteorol. 131, 77–96.
Vermote, E., Vermeulen, A., 1999. Atmospheric Correction Algorithm: Spectral Reflectances (MOD09). ATBD Version, 4.
Wang, T., Peng, S., Lin, X., Chang, J., 2013. Declining snow cover may affect spring phenological trend on the Tibetan Plateau. Proc. Natl. Acad. Sci. 110, E2854–E2855.
Wang, C., Cao, R., Chen, J., Rao, Y., Tang, Y., 2015. Temperature sensitivity of spring vegetation phenology correlates to within-spring warming speed over the Northern Hemisphere. Ecol. Indic. 50, 62–68.
Wang, C., Tang, Y., Chen, J., 2016. Plant phenological synchrony increases under rapid within-spring warming. Sci. Report. 6.
White, M.A., Hoffman, F., Hargrove, W.W., Nemani, R.R., 2005. A global framework for monitoring phenological responses to climate change. Geophys. Res. Lett. 32.
White, M.A., Beurs, D., Kirsten, M., Didan, K., Inouye, D.W., Richardson, A.D., Jensen, O.P., O'Keefe, J., Zhang, G., Nemani, R.R., 2009. Intercomparison, interpretation, and assessment of spring phenology in North America estimated from remote sensing for 1982–2006. Glob. Chang. Biol. 15, 2335–2359.
Wolkovich, E.M., Cook, B., Allen, J., Crimmins, T., Betancourt, J., Travers, S., et al., 2012. Warming experiments underpredict plant phenological responses to climate change. Nature 485, 494–497.
Xia, J., Niu, S., Ciais, P., Janssens, I.A., Chen, J., Ammann, C., Arain, A., Blanken, P.D., Cescatti, A., Bonal, D., 2015. Joint control of terrestrial gross primary productivity by plant phenology and physiology. Proc. Natl. Acad. Sci. 112, 2788–2793.
Xiao, X., Boles, S., Liu, J., Zhuang, D., Liu, M., 2002. Characterization of forest types in Northeastern China, using multi-temporal SPOT-4 VEGETATION sensor data. Remote Sens. Environ. 82, 335–348.
Zhang, Y., Tang, Y., 2005. Inclusion of photoinhibition in simulation of carbon dynamics of an alpine meadow on the Qinghai-Tibetan plateau. J. Geophys. Res. Biogeosci. 2005–2012, 110.
Zhang, X., Friedl, M.A., Schaaf, C.B., Strahler, A.H., Hodges, J.C.F., Gao, F., Reed, B.C., Huete, A., 2003. Monitoring vegetation phenology using MODIS. Remote Sens. Environ. 84, 471–475.
Zhang, X., Friedl, M.A., Schaaf, C.B., 2006. Global vegetation phenology from Moderate Resolution Imaging Spectroradiometer (MODIS): evaluation of global patterns and comparison with in situ measurements. J. Geophys. Res. Biogeosci. 2005–2012, 111.
Zhang, G., Zhang, Y., Dong, J., Xiao, X., 2013. Green-up dates in the Tibetan Plateau have continuously advanced from 1982 to 2011. Proc. Natl. Acad. Sci. 110, 4309–4314.
Zhou, L., Tucker, C.J., Kaufmann, R.K., Slayback, D., Shabanov, N.V., Myneni, R.B., 2001. Variations in northern vegetation activity inferred from satellite data of vegetation index during 1981 to 1999. J. Geophys. Res. 106, 20069.